[h!]

GRAPHICAL ABSTRACT

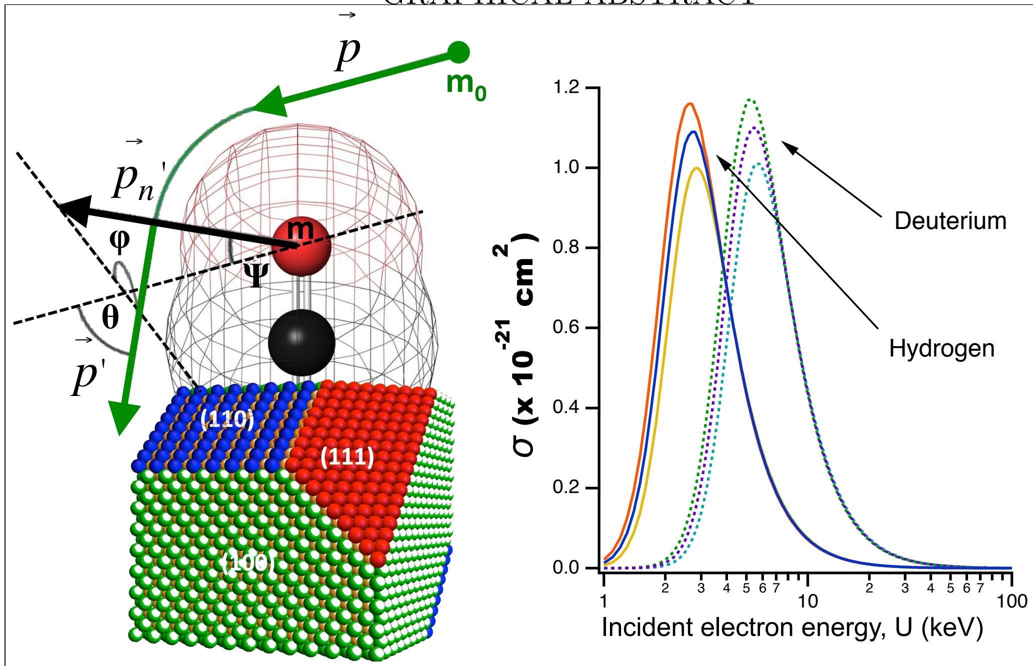

Role of knock-on in electron beam induced etching of diamond

Marco Fronzi[2,*]

School of Mathematical and Physical Sciences, University of Technology, Sydney,P.O. Box 123, Broadway, New South Wales 2007, Australia.

James Bishop[2,**]

School of Mathematical and Physical Sciences, University of Technology, Sydney,P.O. Box 123, Broadway, New South Wales 2007, Australia.

Blake Regan

School of Mathematical and Physical Sciences, University of Technology, Sydney,P.O. Box 123, Broadway, New South Wales 2007, Australia.

M. Hussein N. Assadi

Center for Computational Sciences, University of Tsukuba, Tennodai 1-1-1, Tsukuba, Ibaraki 305-8577, Japan.

Catherine Stampfl

School of Physics, The University of Sydney, Sydney, New South Wales 2006, Australia.

Igor Aharonovich

School of Mathematical and Physical Sciences, University of Technology, Sydney,P.O. Box 123, Broadway, New South Wales 2007, Australia.

Michael J. Ford

School of Mathematical and Physical Sciences, University of Technology, Sydney,P.O. Box 123, Broadway, New South Wales 2007, Australia.

---

[*]Corresponding author
[**]Corresponding author
Email addresses: `marco.fronzi@uts.edu.au` (Marco Fronzi), `James.Bishop@uts.edu.au` (James Bishop)
[1]MF and JB authors equally contributed to the paper
[2]DOI 10.1016/j.carbon.2020.03.039

Milos Toth

School of Mathematical and Physical Sciences, University of Technology, Sydney,P.O. Box 123, Broadway, New South Wales 2007, Australia.

Abstract

Electron beam induced etching (EBIE) has recently emerged as a promising direct-write nanofabrication technique. EBIE is typically assumed to proceed entirely through chemical pathways driven by electron-electron interactions. Here we show that knock-on (i.e., momentum transfer from electrons to nuclei) can play a significant role in EBIE, even at electron beam energies as low as 1.5 keV. Specifically, we calculate knock-on cross-sections for H, D, O and CO on the surface of diamond and show experimentally that they affect the kinetics of EBIE performed using oxygen, hydrogen and deuterium etch precursors. Our results advance basic understanding of electron-adsorbate interactions, particularly in relation to EBIE and the related techniques of electron beam-induced deposition and surface functionalisation.

1. Introduction

The most commonly-used high resolution imaging, analysis and lithography techniques employ electron beams. The beam energy is often selected to either cause or prevent sample modification/damage, and it is assumed that atomic displacements caused by knock-on are negligible below a material-dependent energy threshold. Indeed, transmission electron microscopy (TEM) is routinely performed using energies selected to avoid knock-on displacements, and in scanning electron microscopy (SEM) knock-on is normally assumed to be negligible [1, 2, 3, 4, 5, 6]. Here we show that knock-on processes which are normally assumed to be forbidden at low electron energies due to momentum conservation can occur at energies that are over an order of magnitude lower than expected.

Diamond is a technologically-significant material [7] and a useful model system for studies of electron-driven sample modification – both in TEM studies of diamond restructuring caused by knock-on [3, 4] as well as SEM studies of electron beam induced etching (EBIE) which proceeds primarily

through chemical pathways [5, 8]. In both cases, it is assumed that knock-on processes are negligible at beam energies below approximately 50 keV [3, 4, 5, 8]. Here we show that this assumption is incorrect and knock-on can modify diamond at energies that are over an order of magnitude smaller. Specifically, we use EBIE of diamond to show that knock-on can modify etch kinetics at beam energies as low as 1.5 keV.

EBIE is a direct-write lithography technique in which an electron beam is used to etch materials through reactions that involve surface-adsorbed precursor molecules [5, 8]. It is normally performed by injecting precursor gases into an SEM, and has proved successful in nanofabrication of optical devices such as pillar waveguides [9] and optical dielectric cavities [10] made from diamond and hexagonal boron nitride – materials that are technologically important [7, 11], but difficult to process due to their high chemical and thermal stabilities. EBIE holds significant potential for high reolution nanofabrication and material processing, yet is currently at an early development stage.

SEM EBIE is typically discussed exclusively in terms of chemical mechanisms initiated by collisions between hot electrons (i.e., the electron beam, backscattered electrons and secondary electrons), and thermalised (bonding) electrons at the adsorbate-solid interface. For example, when EBIE of diamond is carried out using O_2 or H_2O as the precursor gas, these mechanisms include electron-stimulated desorption of surface-terminating species (e.g., O, H and OH), dissociation of molecular precursor adsorbates, and desorption of CO formed as a result of chemisorption of O to diamond [5, 8, 12]. Here, we use diamond – the most thoroughly characterised material in the field of EBIE – to demonstrate knock-on displacement of surface species at energies as low as 1.5 keV.

2. Results

2.1. Calculations of knock-on thresholds

Here, we use a semi-classical approach to calculate cross-sections for direct knock-on of chemisorbed CO, O, H and D (deuterium) species from (111), (110) and (100) surfaces by electron impact for electron beam energies between 1 and 100 keV. Knock-on induced desorption of monolayer adsorbates from solid surfaces has been described in detail by Morita[13], for the case of energetic ion bombardment. We assume that knock-on induced desorption

of an adsorbed atom or molecule by electron impact can occur via the same general mechanisms:

- (I): Knock-on by an incoming primary electron followed by reflection of the displaced adsorbate from the substrate surface.
- (II): Knock-on by an outgoing backscattered electron (BSE), imparting momentum in a direction away from the surface.

We calculate the desorption cross-sections for direct knock-on only. These represent desorption via mechanism (II). Cross-sections for desorption via mechanism (I) will be given by multiplication of the cross-sections with a reflection coefficient, between zero and unity, representing the average proportion of displaced atoms that reflect from the surface and desorb. This reflection coefficient depends strongly upon the mass ratio of the displaced adsorbate atom, M_d to the substrate atoms, M_s[13]. The reflection coefficient decreases with increasing M_d/M_s and should be close to unity for H and D on C. Here, a reflection coefficient of unity is assumed for simplicity.

We begin with calculation of the energetically favourable adsorption configurations from which each surface species will desorb, through standard geometry relaxation using density functional theory (DFT). The favoured adsorption configurations were calculated for a single O, H, D or CO adsorbed upon a (100), (110) or (111) unterminated diamond surface as well as surfaces terminated fully with O or with H. Oxygen can adsorb in either the ether or ketone configuration upon diamond while H adsorbs only in the ketone configuration. Oxygen adsorbs favourably in the ketone configuration on (111) and (110) surfaces, and in the ether configuration on the (100) surface. The surface termination was found not to alter the favoured configuration and variation was found only between the crystal planes. The favoured configurations for H and O are shown in Figure 1. Having determined the favourable adsorption configurations, we focus on the desorption of each species from both hydrogen and oxygen terminated surfaces, as schematically depicted in Fig. 2(a) and (b).

We define the knock-on threshold (T_d) as the minimum kinetic energy required to facilitate displacement of a particular atomic or molecular species. T_d can be calculated accurately with computationally expensive molecular dynamics simulations.[14, 2] However, it was suggested by Morita, that the outward potential barrier may be replaced by the adsorption energy of the adsorbates on the substrate. This was sucessively demonstrated conclusively

by Komsa *et al.*, that T_d can be well-approximated by the vacancy formation energy (or desorption energy) calculated for a "frozen" crystal structure[13, 14]. In this approach, DFT is used to calculate the energy difference when a species is removed (desorbed) from the surface while freezing the rest of the atoms of the simulation in their original positions. This is done in place of allowing the system to relax into the lowest energy state after desorption. In this way, T_d can be obtained in a much more computationally efficient manner by computing the desorption energy while preventing geometrical relaxation of the system after vacancy creation. We refer to this as the *"desorption energy calculated under un-relaxed conditions"*.

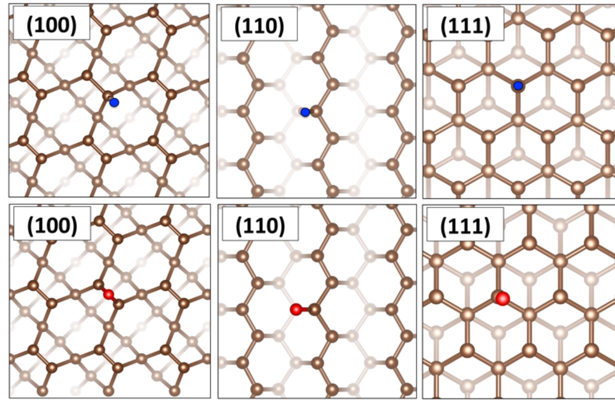

Figure 1: Stable geometries of hydrogen (top) and oxygen atoms, following adsorption on the diamond (111), (110) and (100) surfaces after full atomic relaxation. Oxygen adsorbs favourably in the ether configuration on (100) (bottom left), whereas the other systems favour the ketone configuration. Here, brown, red and blue spheres represent carbon, oxygen and hydrogen atoms, respectively. Here the unterminated surfaces are shown for clarity of the adsorbate yet the configurations are approximately equal on the terminated surfaces.

The *"un-relaxed"* desorption energies, listed in Tab.1, are then calculated as follows:

$$E_{\mathrm{Des}} = (E_{\mathrm{Surf-Des}} + E_{\mathrm{Atom}}) - E_{\mathrm{Surf}} \quad , \tag{1}$$

where E_{Atom} is the total energy of the desorbed species, and E_{Surf} and $E_{\mathrm{Surf-Des}}$ are the total energies of the surface before and after molecular/atomic desorption, respectively, with no geometry relaxation upon desorption. T_d is then approximated as E_{Des}, and the formalism developed by McKinley-Feshbach[15], is used to calculate knock-on cross-sections[14, 15].

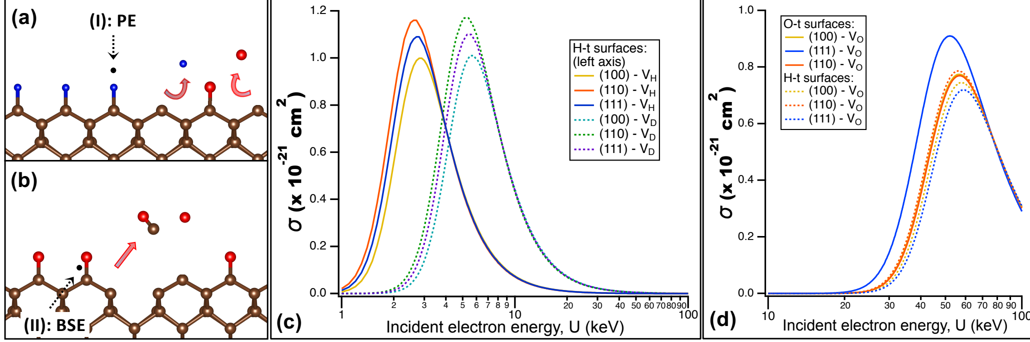

Figure 2: (Color online) Desorption via electron impact induced knock-on of chemisorbates on diamond. (a-b) Schematic illustrations of CO (brown and red), H (blue) and O (red) desorption from a (100) surface terminated by H and/or O. Desorption via mechanism (I), i.e knock-on by an incoming primary electron followed by reflection from the surface is shown in (a). Mechanism (II), direct knock-on induced desorption by a backscattered electron (directed out of the surface) is illustrated in (b). (c) Total cross sections (σ) versus electron energy for knock-on desorption of H and D from H-terminated (100), (110) and (111) surfaces of diamond. (d) Knock-on cross-sections for desorption of O from H-terminated and O-terminated diamond (labelled 'H-t' and 'O-t', respectively).

We calculate Mott electron scattering cross-sections (σ) for knock-on desorption of H, D, O and CO from the (111), (110) and (100) surfaces of diamond[16]. σ was calculated as follows:

$$\sigma = \int_{-\infty}^{+\infty} P(v,T)\sigma_{\mathrm{D}}(T_{max},T_d)\Theta(T_{max}-T_d)dv \tag{2}$$

where $P(v,T)$ is the distribution of probability to find an atom with velocity v at temperature T, Θ is the Heaviside step function, and σ_{D} is the cross-section of the event where the transferred energy is greater than the displacement threshold, and it is given by:

$$\begin{aligned}\sigma_{\mathrm{D}} = \frac{4Z^2E_R^2}{m_e^2c^4}\left(\frac{T_{max}}{T_d}\right)\pi a_0^2\left(\frac{1-\beta^2}{\beta^4}\right)\Bigg\{1+2\pi\alpha\beta\sqrt{\frac{T_d}{T_{max}}} \\ -\frac{T_d}{T_{max}}\left[1+2\pi\alpha\beta+(\beta^2+\pi\alpha\beta)ln\left(\frac{T_{max}}{T_d}\right)\right]\Bigg\} \quad .\end{aligned} \tag{3}$$

Here, Z is the atomic number of the target, E_R is the Rydberg energy, a_0 is the Bohr radius of the hydrogen atom, β velocity of electrons expressed as a fraction of the speed of light, m_e the rest mass of an electron and

$\alpha \approx Z/137$. T_d is the threshold energy for atomic displacement, whereas T_{max} is the effective maximum energy transferred in a collision that takes into account the vibrational motion of the nucleus, and is defined as:

$$T_{max}(v, E) = \frac{(r + \frac{t}{c})^2}{2m_n} \quad , \tag{4}$$

where m_n is the mass of the target nucleus. Here, r and t are defined as:

$$r = \frac{1}{c}\sqrt[2]{E(E + 2m_e c^2)} + m_n v \quad , \tag{5}$$

and

$$t = \sqrt[2]{E + E_n(E + 2m_e c^2 + E_n)} \quad , \tag{6}$$

with v and E_n the velocity and kinetic energy of the target atom. A formal derivation of the above equations can be found in ref. [2]. To calculate the knock-on cross-sections for specific atomic and molecular species on different surfaces of diamond, we approximate T_d by the desorption energy (E_d), which was calculated using density functional theory (DFT), as is detailed in Section 4, and we set $T = 300$K to be consistent with the experimental data.

Table 1: H, O and CO desorption energies (E_d) calculated under *"un-relaxed"* conditions for the oxygen terminated (O-t) and hydrogen terminated (H-t) (100), (110) and (111) surfaces. Here, we also show the desorption energy on selected pristine, unterminated surfaces for completeness.The energies are calculated with respect to the free carbon monoxide, atomic oxygen and atomic hydrogen in the gas phase.

	E_d (eV)		
Desorbed species	(111)	(110)	(100)
H-t-V_O	6.17	5.87	6.05
H-t-V_H	4.85	4.24	4.60
H-t-V_{CO}	5.65	5.26	6.06
O-t-V_O	5.41	5.94	5.92
O-t-V_H	4.40	4.28	4.68
O-t-V_{CO}	4.37	2.72	6.15
V_O	5.75	7.49	6.00
V_H	4.35	4.21	4.55
V_{CO}	3.77	5.36	5.48

Table 1 shows the calculated values of E_d for O, H and CO on the (111), (110) and (100) diamond surfaces terminated by O and H. Fig. 2(c) then shows the cross-sections for knock-on, σ of H and D, calculated using the E_d value for H, on surfaces terminated by H. Fig. 2(d) shows σ for the desorption of O from surfaces terminated by O and H. Each cross-section is negligible below a threshold defined by momentum conservation, and its maximum increases with atomic mass and the binding energy [4]. The cross-section for desorption of H peaks at $\sim$2.7 keV, and does not vary substantially with surface type as the binding energies for H (Table 1) are similar on all surfaces considered. The knock-on cross-sections for D are negligible below $\sim$ 2 keV, and peak at $\sim$5 keV. The shift to higher energy is due to the differing mass of the isotopes (which have equivalent chemical properties and hence the same calculated bond strengths and desorption energies). The oxygen cross-sections have a maximum at $\sim$ 50 keV, and are negligible below $\sim$ 20 keV. As a result of the difference between the H and D cross-sections seen in Fig. 2(c), we expect preferential knock-on desorption of H (significant for H, negligible for D) at electron beam energies between 1 and 2 keV.

2.2. Electron beam induced etching of diamond

To test this prediction, we performed EBIE of diamond using H_2, D_2 and O_2 precursor gases. Figures 3 (a) and (b) show SEM images of two regions of (100)-oriented diamond that were etched using an electron beam energy of 1.5 keV, and a 2:1 partial pressure of H_2:O_2 and D_2:O_2, respectively. The images show surface topographies generated by EBIE that are anisotropic, meaning that the etch rate depends on crystallographic direction[3].

Previously, we determined that in the case of diamond EBIE performed using a mixture of H_2 and O_2, the coverage ratio of adsorbed H:O naturally varies between crystal planes as a result of plane-dependent variation in the adsorption energy of O [12]. It decreases in the order {110} >{111} >{100}, and as a result, affects the geometry of the topographic patterns as the etch rate of O-terminated diamond is much greater than that of H-terminated diamond. This makes *the etch rate in a specific crystal direction inversely proportional to the H:O coverage ratio on the plane normal to that direction.* [4] In addition, previously calculated desorption energies of CH_x and CO_x

[3]Fast-etching planes are absent from images, and patterns are dominated by the slowest etching planes [8]

[4]High-energy “edge-sites”, such as step-edges and defects, may play a role in EBIE

species from diamond were found to be far higher for CH_x, resulting in a lower desorption rate for CH_x species for desorption via secondary electron induced bond scission. This is the primary mechanism driving EBIE and explains the higher etch rate observed for EBIE using O_2 vs H_2[12]. The far higher desorption energy of CH_x also means that knock-on cross-sections will be negligible below 30 keV and were therefore not calculated.

The images in Fig. 3 show that the topographic patterns (magnified in the insets) differ when D_2 is used in place of H_2. Specifically, the topography consists exclusively of inverted pyramids with smooth {111} sidewalls (features of type '1' labelled in Fig. 3(b) and magnified in the inset). Conversely, in the case of H_2, the patterns are less symmetric and the pyramids contain both {110} facets and {111} facets (see the features labelled '2' & '3' and the inset in Fig. 3(a)). The reduced symmetry is also evident in Fourier transforms of the images, also shown in Fig. 3. The difference between the transforms reflects that image contrast, in the case of D_2, is dominated by horizontal, vertical and diagonal lines (i.e., facet edges), whereas the contrast is more radially-uniform in the case of H_2. We attribute the difference in pattern geometry to preferential knock-on desorption of H over D, as expected from the cross-sections in Fig. 2 (the cross-sections also show that knock-on desorption of O is negligible at energies below $\sim$ 20 keV and therefore does not play a role at the beam energy of 1.5 keV used in this experiment). The isotope-resolved data in Figure 3 serve as evidence that knock-on desorption can indeed play a role in EBIE even at an electron beam energy as low as 1.5 keV.

We note that the net etch rates vary considerably for the different precursor combinations. EBIE with pure O_2 is fastest, it is lower for $H_2 + O_2$ (as reported previously [12]) and significantly lower still for $D_2 + O_2$. This difference between H_2 and D_2 is strong additional evidence for preferential desorption of H via knock-on – i.e., by desorbing hydrogen, surface sites become available for chemisorption of oxygen which elevates the etch rate.

Next, we turn to knock-on desorption of CO. Figure 4(a) shows the cross-sections for knock-on desorption of CO on O and H-terminated surfaces of diamond. The cross-sections are negligible below 30 keV, except for the

via reduced energy barriers for electron induced desorption of etch products at such sites. However, we expect edge sites to display the same qualitative trends as the crystal planes and desorption energies for CH/D_x to be higher than for CO_x, i.e H/D adsorption always passivates sites relative to O adsorption.

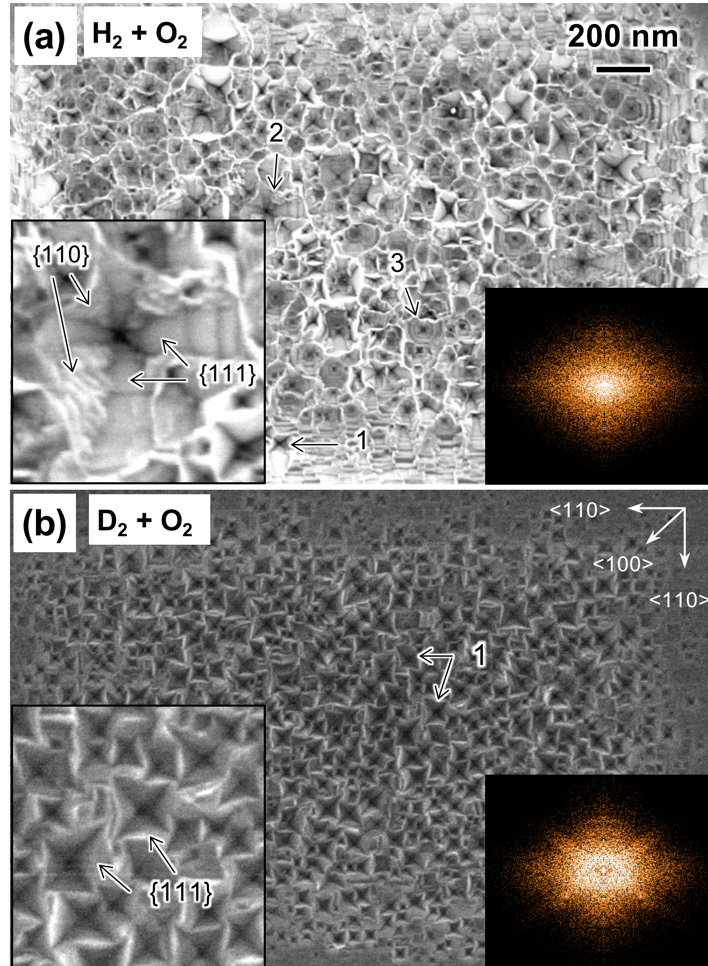

Figure 3: (Color online) Topographic patterns formed in (100) diamond by EBIE performed using an electron beam energy of 1.5 keV, and a 2:1 mix of (a) H_2:O_2, and (b) D_2:O_2. A number of topographic features are labelled '1' - '3' in the images. The inset in (a) shows a magnified view of a feature of type '2' which is present only in the case of H_2. The corresponding inset in (b) shows a magnified view of features of type '1' which are present in both images. The insets on the right are Fourier transforms of the images. Differences between the pattern geometries seen in (a) and (b) are attributed to preferential knock-on desorption of H. The scale bar and crystal directions apply to both images.

case of the O-terminated (110) surface, where σ becomes significant at $\sim$ 15 keV, and has a maximum at $\sim$ 40 keV. Desorption of CO is believed to be a primary mechanism for EBIE of diamond [12], but it is generally

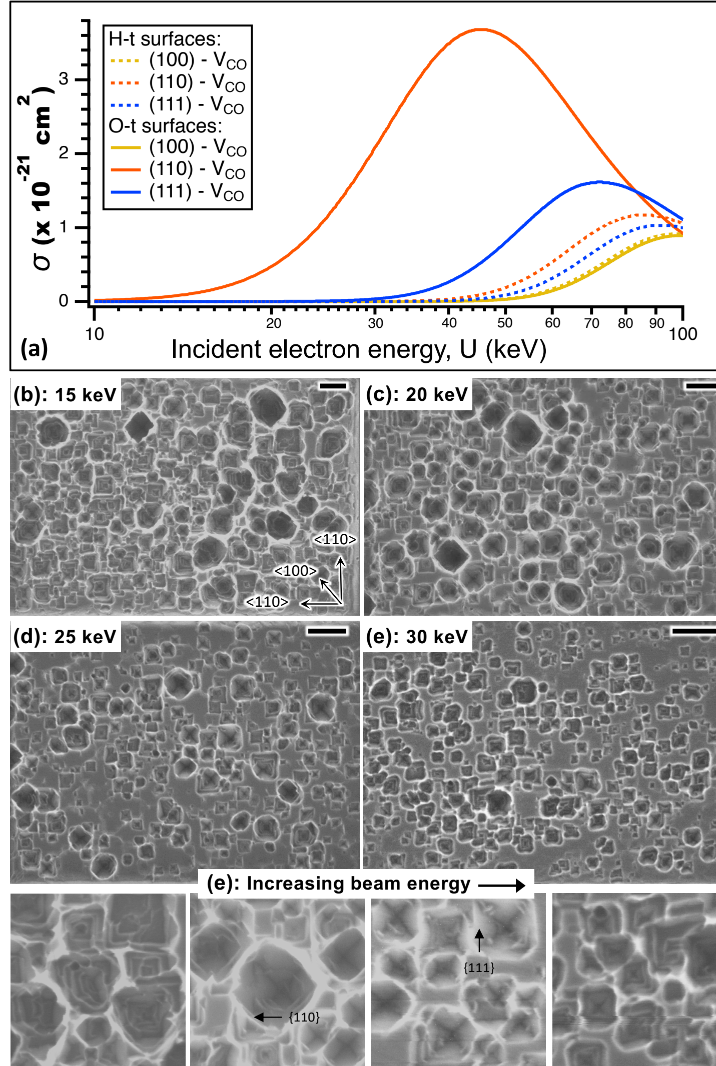

Figure 4: (Color online) (a) Cross-sections for knock-on desorption of CO from diamond terminated by H ('H-t') and O ('O-t'). (b - e) Topography of (100) diamond etched with O_2 precursor gas using electron beam energies of 15, 20, 25 and 30 keV. The etched surfaces between the inverse pyramids (with {111} side-walls) become smoother while the occurrence of edges aligned with <100> directions ({110} plane remnants) decreases with increasing beam energy. (e) Higher magnification images of key pattern features found in the etch pits shown in (b - e) highlighting the decreasing occurence of <100> aligned features, attributed to an increasing etch rate for {110} planes due to knock-on of CO. Scale bars are 200 nm. Crystal directions shown in (b) apply to all images.

believed to proceed exclusively through bond scission caused by electron-electron scattering. The cross-sections in Fig. 4(a) indicate that a knock-on contribution is expected for EBIE of the (110) plane at electron energies greater than $\sim$ 15 keV. To test this hypothesis, we performed EBIE using electron beam energies greater than 10 keV and O_2 as the precursor gas. Figure 4(b-e) shows images of diamond regions that were etched using beam energies of 15, 20, 25 and 30 keV. As the beam energy is increased, the abundance of {100} planes (seen as smooth, flat regions between the pits in Fig. 4) is increased and remnants of {110} planes decreased[5] due to knock-on desorption of CO from the {110} plane and hence accelerated etching of that plane. The change in topography observed here is more subtle than that seen in Fig. 3 because the increase in electron energy from 15 to 30 keV modifies the rates of numerous (chemical and knock-on) mechanisms that contribute to EBIE. The change seen in the images is, however, consistent with the cross-sections for knock-on desorption of CO shown in Fig. 4(a) because an increase in the etch rate of the {110} plane is expected to suppress the presence of that plane and increase the abundance of the slower etching {100} and {111} planes.

3. Conclusions

In conclusion, we demonstrated that knock-on desorption of chemisorbates plays a role in EBIE of diamond at electron beam energies as low as 1.5 keV. Our results improve present understanding of mechanisms responsible for electron restructuring of surfaces, and will aid the design and optimisation of EBIE processes. Our findings are also relevant to the related techniques of electron beam induced surface functionalisation/activation and electron beam induced deposition [5, 17, 18, 19], in which knock-on desorption of species such as H, O and OH can affect surface structure and deposit purity.

[5]Remnants of {110} planes manifest primarily as edges aligned with <100> directions in the topographic patterns. These are more abundant for a slower etch rate of the {110} plane.

4. Methodology

4.1. Calculation Methods

We perform density functional theory (DFT) calculations, with the generalized gradient approximation (GGA) for the exchange-correaltion functional, in particular that of Perdew-Burke-Ernzerhof (PBE)[20]. We use periodic boundary conditions and a localized atomic orbital basis set as implemented in the SIESTA code, where the core-valence interaction is described by norm coneserving pseudopotentials[21, 22]. Double-zeta plus polarization orbitals (DZP) are used, and the cut-off energy for the valence electrons is 750 Ry[22]. Γ point calculations have been used for (3×4), (3×4) and (4×4) surface unit cell of the (111), (110) and (100) surfaces, consisting of 12 atomic layers, with a vacuum region of ∼25 Å. Full geometry optimization has been carried out for each system, and the convergence criteria for the energy and forces are 10^{-5} eV and 10^{-2} eV/ Å, respectively.

4.2. Diamond samples

The sample used for EBIE was a (100) oriented single-crystal diamond membrane of ∼ 5 μm thickness. This is prepared using the method detailed in references 23, 24, 25. Briefly, ion implantation is used to form a damaged, graphitized layer at ∼ 1.7 μm depth within a commercially purchased (Element 6), polished, CVD grown, type 2a (100) single-crystal diamond. Electrochemical etching is then used to etch away the graphitized layer, resulting in liftoff of the ∼ 1.7 μm thick top layer. This thin diamond layer is then isolated and transferred to a silicon substrate. This thin membrane is then used as the substrate for epitaxial growth of a fresh layer of single crystal diamond.

The fresh layer of single-crystal diamond is grown epitaxially using a commercial (ASTEX), microwave plasma enhanced CVD reactor, with a 1 % mix of CH_4 in H_2 and 900 W of microwave power for 45 minutes. This resulted in a layer of ∼ 3 μm thickness. All pits were etched within this layer. The overgrown layer is of high crystalline quality and has a low impurity concentration. The diamond grown in our reactor in this manner reproducibly has high optical transmission across the visible spectrum (optically clear). It also has a very low intensity of photo-luminscence emissions when excited with a 532 nm laser indicating that nitrogen and silicon impurities are low.

Immediately after growth, the fresh diamond surface is clean and suitable for direct insertion into the SEM for EBIE experiments. In this way, rigorous

cleaning procedures that are normally necessary for reproducible EBIE [12] can be foregone. Furthermore, the utilization of fresh diamond grown in this "bottom-up" manner avoids the presence of a "damage-layer" that is found at the surface of commercial samples that have been polished. This damage-layer is typically 1−2 μm thick and is caused by the polishing procedures. We observe that EBIE behaviour is altered within this layer when using bulk diamonds obtained commercially, even with high quality "electronic grade" diamond. Etch rates are faster within the damage layer and topographic patterns form only partially, or are not observed at all within the damage layer – this explains some differences between surface topography of diamond etched by O_2 reported in the present work and in Ref. [12].

4.3. Electron beam induced etching methodology

EBIE was peformed using an FEI Sirion Field emission gun SEM, that has been modified for variable pressure operation. Precursor gases fill the entire SEM chamber at the partial pressures indicated. The electron beam current was set to 10.7 nA for all etches. An etch frame of 2.42 x 1.82 μm (7.81 μm^2), resulting in a primary electron flux of $\sim 8.6 \times 10^9$ electrons/μm^2.s, was used for all etches. The beam scan used was the native analog raster pattern of the SEM with 1.67 ms time per line and 484 lines per frame.

The total chamber pressure for each etch was ∼ 23.2 Pa composed of a 2:1 partial pressure ratio mixture of either H_2:O_2 or D_2:O_2, or just pure O_2 at ∼ 7.7 Pa. An RF remote plasma generator was active during all etches at 13.9 MHz, 5W load power in order to radicalize the precursor gases as described in Ref. [12]. Etch durations were both 15 minutes for the pits shown in Fig. 3. For the etch pits shown in Fig. 4, etch durations were adjusted according to the beam energy dependent etch rate (estimated beforehand by etching pits of constant duration and estimating etched volume at each energy). Etch durations in Fig. 4 were approximately 15, 18, 22 and 27 mins for beam energies of 15, 20, 25 and 30 keV.

The sample was loaded into the SEM immediately after growth of the diamond layer. Plasma cleaning of the chamber is then performed overnight with O_2 gas at 13 Pa, 5W load power, using the same RF remote plasma generator used during EBIE. This minimizes any residual water or organic contaminants that can interfere with EBIE of diamond. The gases used were all high purity (>99.99 %, Sigma-Aldrich) and are delivered to the SEM chamber via a leak-free system (confirmed with He leak testing). All lines are heated to 60 °C at all times to aid desorption of gases. They are flushed

extensively with dry N_2 prior to precursor gas flow and when changing gas combinations. Finally, the gases flow through a cold trap held at -116 °C prior to entering the chamber, in order to further purify the gas stream.

5. Acknowledgements

The authors gratefully acknowledge the financial support of the National Natural Science Foundation of China (No. 51323011), and the Australian Government through the Australian Research Council (ARC DP160101301, DP180100077, DP190101058, LP170100150). Theoretical calculations were undertaken with the assistance of resources from the National Computational Infrastructure (NCI), which is supported by the Australian Government, and resources provided by the Pawsey Supercomputing Centre with funding from the Australian Government and the Government of Western Australia. MF and JB contributed equally to this work.

References

[1] O. Dyck, M. Ziatdinov, D. B. Lingerfelt, R. R. Unocic, B. M. Hudak, A. R. Lupini, S. Jesse, S. V. Kalinin, Atom-by-atom fabrication with electron beams, Nat. Rev. Mater. 4 (2019) 497–507.

[2] J. C. Meyer, F. Eder, S. Kurasch, V. Skakalova, J. Kotakoski, H. J. Park, S. Roth, A. Chuvilin, S. Eyhusen, G. Benner, A. V. Krasheninnikov, U. Kaiser, Accurate Measurement of Electron Beam Induced Displacement Cross Sections for Single-Layer Graphene, Phys. Rev. Lett. 108 (2012) 196102.

[3] A. V. Krasheninnikov, F. Banhart, Engineering of nanostructured carbon materials with electron or ion beams, Nat. Mater. 6 (2007) 723–733.

[4] F. Banhart, Irradiation effects in carbon nanostructures, Rep. Prog. Phys. 62 (1999) 1181–1221.

[5] I. Utke, S. Moshkalev, P. Russell, Nanofabrication Using Focused Ion and Electron Beams: Principles and Applications, Oxford University Press, USA, 2012.

[6] R. F. Egerton, P. Li, M. Malac, Radiation damage in the TEM and SEM, Micron 35 (2004) 399–409.

[7] M. Atatüre, D. Englund, N. Vamivakas, S.-Y. Lee, J. Wrachtrup, Material platforms for spin-based photonic quantum technologies, Nat. Rev. Mater. 3 (2018) 38–51.

[8] A. A. Martin, A. Bahm, J. Bishop, I. Aharonovich, M. Toth, Dynamic Pattern Formation in Electron-Beam-Induced Etching, Phys. Rev. Lett. 115 (2015) 255501–5.

[9] A. A. Martin, M. Toth, I. Aharonovich, Subtractive 3D printing of optically active diamond structures, Sci. Rep. 4 (2014) 5022.

[10] S. Kim, J. E. Fröch, J. Christian, M. Straw, J. Bishop, D. Totonjian, K. Watanabe, T. Taniguchi, M. Toth, I. Aharonovich, Photonic crystal cavities from hexagonal boron nitride, Nat. Commun. 9 (2018) 2623.

[11] K. K. Kim, H. S. Lee, Y. H. Lee, Synthesis of hexagonal boron nitride heterostructures for 2d van der waals electronics, Chem. Soc. Rev. 47 (2018) 6342–6369.

[12] J. Bishop, M. Fronzi, C. Elbadawi, V. Nikam, J. Pritchard, J. E. Fröch, N. M. H. Duong, M. J. Ford, I. Aharonovich, C. J. Lobo, et al., Deterministic nanopatterning of diamond using electron beams, ACS Nano 12 (2018) 2873–2882.

[13] K. Morita, D. Ishikawa, R. Ishigami, J. Yuhara, K. Soda, Ion impact desorption of monolayer adsorbates on solid surfaces, Izvestiya Akademii Nauk. Rossijskaya Akademiya Nauk. Seriya Fizicheskaya 62 (1998) 2468–2478.

[14] H.-P. Komsa, J. Kotakoski, S. Kurasch, O. Lehtinen, U. Kaiser, A. V. Krasheninnikov, Two-Dimensional Transition Metal Dichalcogenides under Electron Irradiation: Defect Production and Doping, Phys. Rev. Lett. 109 (2012) 035503.

[15] W. A. Mckinley, H. Feshbach, The Coulomb Scattering of Relativistic Electrons by Nuclei, Physical Review 74 (1948) 1759.

[16] N. F. Mott, The Scattering of Fast Electrons by Atomic Nuclei , Proc. Royal Soc. A 124 (1929) 425.

[17] T. W. Shanley, A. A. Martin, I. Aharonovich, M. Toth, Localized chemical switching of the charge state of nitrogen-vacancy luminescence centers in diamond, Appl. Phys. Lett. 105 (2014) 063103.

[18] M. Walz, M. Schirmer, F. Vollnhals, T. Lukasczyk, H. P. Steinruck, H. Marbach, Electrons as "Invisible Ink": Fabrication of Nanostructures by Local Electron Beam Induced Activation of SiOx, Angew. Chem. Int. Edit. 49 (2010) 4669–4673.

[19] K. Muthukumar, H. O. Jeschke, R. Valentí, E. Begun, J. Schwenk, F. Porrati, M. Huth, Spontaneous dissociation of $Co_2(CO)_8$ and autocatalytic growth of Co on SiO_2: A combined experimental and theoretical investigation, Beilstein J. Nanotechnol. 3 (2012) 546–555.

[20] J. P. Perdew, K. Burke, M. Ernzerhof, Generalised gradient approximation made simple, Phys. Rev. Lett. 77 (1996) 3865.

[21] J. M. Soler, E. Artacho, J. D. Gale, A. García, J. Junquera, P. Ordejón, D. Sánchez-Portal, The SIESTA method for ab initio order-N materials simulation, Journal Physics: Condensed Matter 14 (2002) 2745.

[22] D. R. Hamann, M. Schlüter, C. Chiang, Norm-Conserving Pseudopotentials, Phys. Rev. Lett. 43 (1979) 1494.

[23] K. Bray, B. Regan, A. Trycz, R. Previdi, G. Seniutinas, K. Ganesan, M. Kianinia, S. Kim, I. Aharonovich, Single crystal diamond membranes and photonic resonators containing germanium vacancy color centers, ACS Photonics 5 (2018) 4817–4822.

[24] A. P. Magyar, J. C. Lee, A. M. Limarga, I. Aharonovich, F. Rol, D. R. Clarke, M. Huang, E. L. Hu, Fabrication of thin, luminescent, single-crystal diamond membranes, Applied Physics Letters 99 (2011) 081913.

[25] J. C. Lee, I. Aharonovich, A. P. Magyar, F. Rol, E. L. Hu, Coupling of silicon-vacancy centers to a single crystal diamond cavity, Optics express 20 (2012) 8891–8897.